Published in final edited form as:
Mol Pharm. 2012 August 6; 9(8): 2339–2349. doi:10.1021/mp300277f.

Multimodality Imaging of Breast Cancer Experimental Lung Metastasis with Bioluminescence and a Monoclonal Antibody Dual-Labeled with ^{89}Zr and IRDye 800CW

Hao Hong[1,6], **Yin Zhang**[2,6], **Gregory W. Severin**[2], **Yunan Yang**[1], **Jonathan W. Engle**[2], **Gang Niu**[3], **Robert J. Nickles**[2], **Xiaoyuan Chen**[3], **Bryan R. Leigh**[4], **Todd E. Barnhart**[3], and **Weibo Cai**[1,2,5,*]

[1]Department of Radiology, University of Wisconsin - Madison, WI, USA

[2]Department of Medical Physics, University of Wisconsin - Madison, WI, USA

[3]Laboratory of Molecular Imaging and Nanomedicine, National Institute of Biomedical Imaging and Bioengineering, National Institutes of Health, Bethesda, MD, USA

[4]TRACON Pharmaceuticals, Inc., San Diego, CA, USA

[5]University of Wisconsin Carbone Cancer Center, Madison, WI, USA

Abstract

Metastatic breast cancer is incurable. The goal of this study was to develop a positron emission tomography (PET)/near-infrared fluorescent (NIRF) probe for imaging of CD105 expression in breast cancer experimental lung metastasis. TRC105, a chimeric anti-CD105 antibody, was dual-labeled with a NIRF dye (IRDye 800CW) and ^{89}Zr to yield ^{89}Zr-Df-TRC105-800CW. Luciferase-transfected 4T1 murine breast cancer cells were injected intravenously into female mice to establish the tumor model. Bioluminescence imaging (BLI) was carried out to non-invasively monitor the lung tumor burden. PET imaging revealed that 4T1 lung tumor uptake of ^{89}Zr-Df-TRC105-800CW was 8.7±1.4, 10.9±0.5, and 9.7±1.1 %ID/g at 4, 24, and 48 h post-injection (n = 4), with excellent tumor contrast. Biodistribution studies, blocking, control studies with ^{89}Zr-Df-cetuximab-800CW, ex vivo BLI/PET/NIRF imaging, and histology all confirmed CD105 specificity of the tracer. Broad clinical potential of TRC105-based agents was shown in many tumor types, which also enabled early detection of small metastasis and intraoperative guidance for tumor removal.

Keywords

Breast cancer; lung metastasis; positron emission tomography (PET); near-infrared fluorescence (NIRF); tumor angiogenesis; CD105 (endoglin); ^{89}Zr

Requests for reprints: Weibo Cai, PhD, Departments of Radiology and Medical Physics, University of Wisconsin - Madison, Room 7137, 1111 Highland Avenue, Madison, WI 53705, USA, wcai@uwhealth.org; Phone: 608-262-1749; Fax: 608- 265-0614.
[6]These authors contributed equally to this work

ASSOCIATED CONTENT

Supporting Information

PET imaging and histological examination of CD105 expression in various xenograft tumor models. This material is available free of charge via the Internet at http://pubs.acs.org.

Disclosure of Potential Conflicts of Interest

B.R.L. is an employee of TRACON Pharmaceuticals, Inc. The other authors declare that they have no conflict of interest.

INTRODUCTION

Metastases are the cause of 90% of human cancer deaths.[1] With 230,480 estimated new cases in 2011, breast cancer is the most common malignant disease for women in the United States.[2] Breast cancer patients frequently develop metastases, preferentially to the lung, liver, and bones.[3] The development and clinical translation of novel molecular imaging agents can significantly improve the management of metastatic breast cancer patients through early (metastatic) lesion detection, patient selection/stratification for molecularly-targeted therapies, surgical guidance during tumor resection, treatment monitoring, as well as facilitating new anti-cancer drug development.

One of the core hallmarks of cancer is angiogenesis.[4] It is now generally recognized that angiogenesis is important not only during the rapidly growing macroscopic stage, but also in the microscopic premalignant phase of neoplastic progression and metastasis. Transforming growth factor β (TGF-β) is closely associated with the metastasis of breast cancer cells to the lung.[5, 6] Furthermore, new data continue to emerge on the functional role of CD105 (also called endoglin) within the TGF-β signaling pathway, such as its modulation of cellular responses to TGF-β and its involvement in vascular physiology and angiogenesis.[7] Almost exclusively expressed on proliferating tumor endothelial cells, CD105 is an ideal marker for tumor angiogenesis.[7–9] Clinically, CD105 expression correlates with poor prognosis in more than 10 solid tumor types, including breast cancer.[10] Similarly, our pilot studies revealed high CD105-mediated uptake of radiolabeled TRC105 (an anti-CD105 antibody as described below) in various xenograft tumor models such as triple-negative breast cancer, pancreatic cancer, prostate cancer, and brain tumor (Supplementary Figure 1), which demonstrated broad potential for future application of CD105-targeted agents in cancer imaging and therapy, since all solid tumors depend on angiogenesis and CD105 is overexpressed in most of these tumor types.[4, 10] Therefore, CD105 holds tremendous clinical potential as a prognostic, diagnostic, and therapeutic vascular target in metastatic (breast) cancer.

TRC105 is a human/murine chimeric IgG1 monoclonal antibody (mAb) which binds to both human and murine CD105 and has a very high avidity (with a K_D of 2 ng/mL) for human CD105.[8] A multicenter Phase 1 first-in-human dose-escalation trial was recently completed in the United States and Phase 2 therapy trials are underway in patients with advanced or metastatic ovarian, prostate, bladder, and hepatocellular cancer.[11] These promising clinical data warrant the development of TRC105-based imaging agents, which can play important roles in multiple facets of cancer patient management.

Positron emission tomography (PET) imaging has been widely used in clinical oncology for tumor staging and for monitoring therapeutic efficacy.[12–16] High resolution PET scanners continue to be developed and made available for imaging small animals, improving the capacity for in vivo studies in mice, primates, and humans. This will facilitate cross-species comparisons, which are critical for successful clinical translation and optimal benefit from research using experimental model systems.[17, 18] Recently, mAbs labeled with ^{89}Zr (a positron emitter with a decay half-life of 3.3 days) have gained significant interest, both in preclinical research and in the clinical setting.[19–21]

Optical imaging can complement PET, for example, as an aid to tumor resection.[22–24] For in vivo applications, imaging in the near-infrared (NIR, 700 – 900 nm) region is optimal, since the absorbance spectra for all biomolecules reach minima thus providing a clear optical window for small animal studies and various clinical scenarios (e.g. breast imaging, endoscopy, surgical guidance, etc.).[25–27] In addition to better tissue penetration of light, there is also significantly less tissue autofluorescence in the NIR window. PET/optical

imaging, using a single contrast agent, can provide complementary information that neither modality alone can offer.[24, 28–30] One clinical scenario where such a dual-labeled imaging agent is particularly useful is through the use of initial whole-body PET scan to identify the location of tumor(s), and NIR fluorescence (NIRF) imaging subsequently to guide tumor resection.

In this study, we labeled TRC105 with both ^{89}Zr (via a bifunctional chelator *p*-isothiocyanatobenzyl-desferrioxamine B [Df-Bz-NCS]) and an NIRF dye (IRDye 800CW which has an emission maximum of 806 nm, Figure 1) for dual-modality PET/NIRF imaging of CD105 expression in a breast cancer experimental lung metastasis model. Cetuximab, an isotype matched control mAb which binds to human epidermal growth factor receptor (EGFR) with no cross-reaction to murine tissue,[31] was used as a control. To non-invasively monitor the tumor growth in the murine lung, 4T1 murine breast cancer cells were stably transfected with firefly luciferase (denoted as fLuc-4T1) to enable serial bioluminescence imaging (BLI).[32]

EXPERIMENTAL SECTION

Chemicals and Reagents

TRC105 was provided by TRACON pharmaceuticals Inc. (San Diego, CA) and cetuximab was from Bristol-Myers Squibb Company (Princeton, NJ). AlexaFluor488- and Cy3-labeled secondary antibodies were purchased from Jackson Immunoresearch Laboratories, Inc. (West Grove, CA). Df-Bz-NCS (Macrocyclics, Inc., Dallas, TX), Chelex 100 resin (50–100 mesh, Sigma-Aldrich, St. Louis, MO), IRDye 800CW-NHS ester (LI-COR Biosciences Co., Lincoln, NE), D-Luciferin (Gold BioTechnology, St Louis, MO), and PD-10 desalting columns (GE Healthcare, Piscataway, NJ) were all acquired from commercial sources. Water and all buffers were of Millipore grade and pre-treated with the Chelex 100 resin to ensure that the aqueous solution was heavy metal-free. All other reaction buffers and chemicals were purchased from Thermo Fisher Scientific (Fair Lawn, NJ).

Cell Culture and Animal Model

4T1, MCF-7, and human umbilical vein endothelial cells (HUVECs) were purchased from American Type Culture Collection (ATCC, Manassas, VA). Details for stable transfection of 4T1 cells with firefly luciferase has been described previously.[32] fLuc-4T1 and MCF-7 cells were maintained in RPMI 1640 medium (Invitrogen, Carlsbad, CA) supplemented with 10% fetal bovine serum at 37°C with 5% CO_2. HUVECs were cultured in M-200 medium (Invitrogen, Carlsbad, CA) with 1× low serum growth supplement (Cascade Biologics, Portland, OR) at 37 °C with 5% CO_2. Cells were used when they reached ~75% confluence.

All animal procedures were performed according to a protocol approved by University of Wisconsin - Madison Institutional Animal Care and Use Committee. The fLuc-4T1 breast cancer experimental lung metastasis model was established by intravenous (i.v.) injection of 2×10^5 fLuc-4T1 cells in 100 μL of PBS into 6-week-old female BALB/C mice (Harlan). BLI signal of the mice was monitored regularly using an IVIS Spectrum system (Caliper Life Sciences). Mice were used for PET/NIRF imaging studies when the BLI signals from the thoracic area of mice were substantially strong (typically 3 weeks after inoculation).

MAb-Conjugation and ^{89}Zr-Labeling

^{89}Zr-oxalate was produced using a cyclotron according to the literature procedure with minor modifications.[33, 34] Detailed procedures for Df/800CW conjugation to mAbs and subsequent ^{89}Zr-labeling were similarly to those reported previously.[35, 36] In brief, TRC105 or cetuximab was mixed with Df-Bz-NCS at pH 9.0 at a molar ratio of 1:3 (Figure 1). The

resulting Df-TRC105 and Df-cetuximab were purified with size exclusion chromatography. Afterwards, Df-TRC105 or Df-cetuximab was reacted with 800CW-NHS ester at pH 8.5 with a molar ratio of 1:2. The resulting Df-TRC105-800CW and Df-cetuximab-800CW were purified using PD-10 columns.

For ^{89}Zr-labeling, 74–148 MBq of ^{89}Zr-oxalate was neutralized with a 2 M Na_2CO_3 solution and added to a solution of Df-TRC105-800CW or Df-cetuximab-800CW, where 0.25 mg of mAb conjugate was used per 37 MBq of ^{89}Zr. The total reaction volume was adjusted to 2 mL with 0.5 M HEPES buffer (pH 7.1–7.3), and the reaction mixture (pH 6.8–7.2) was incubated for 1 h at room temperature (RT) with constant shaking. ^{89}Zr-Df-TRC105-800CW and ^{89}Zr-Df-cetuximab-800CW were purified using PD-10 columns, and the radioactive fractions containing ^{89}Zr-Df-TRC105-800CW or ^{89}Zr-Df-cetuximab-800CW were collected and passed through a 0.2 μm syringe filter for in vivo experiments.

Flow Cytometry

The immunoreactivity of TRC105 and Df-TRC105-800CW to HUVECs (high CD105 expression) and MCF-7 (CD105-negative) cells was evaluated by fluorescence-activated cell sorting (FACS) analysis. Cells were harvested and suspended in cold PBS with 2% bovine serum albumin at a concentration of 5×10^6 cells/mL. After incubation with TRC105 or Df-TRC105-800CW (1, 5, or 10 μg/mL) for 30 min at RT and washed three times with cold PBS, the cells were incubated with AlexaFluor488-labeled goat anti-human IgG for 30 min at RT. Afterwards, the cells were washed and analyzed by FACS using a BD FACSCalibur 4-color analysis cytometer, which is equipped with 488 nm and 633 nm lasers (Becton-Dickinson, San Jose, CA) and FlowJo analysis software (Tree Star, Inc., Ashland, OR).

Imaging and Biodistribution Studies

PET and PET/CT scans at various time points post-injection (p.i.), image reconstruction, and region-of-interest (ROI) analysis were performed using a microPET/microCT Inveon rodent model scanner (Siemens Medical Solutions USA, Inc.) as detailed previously.[34] Each fLuc-4T1 tumor-bearing mouse was injected with 5–10 MBq of the PET tracer (which contained 300 picomole of conjugated 800CW dye) via tail vein and 3–15 min static PET scans were performed. Quantitative data were presented as percentage of injected dose per gram of tissue (%ID/g; mean ± SD). A cohort of four fLuc-4T1 tumor-bearing mice was each injected with 2 mg of unlabeled TRC105 at 2 h earlier than ^{89}Zr-Df-TRC105-800CW administration to evaluate the CD105 specificity of ^{89}Zr-Df-TRC105-800CW in vivo (i.e. blocking experiment). NIRF imaging was performed with a Pearl Impulse scanner (LI-COR, Inc., Lincoln, NE) using the 800 nm/white channels, while BLI was carried out in the IVIS Spectrum system after intraperitoneal (i.p.) injection of D-luciferin (150 mg/kg mouse body weight). Biodistribution studies were carried out after the last PET scans to validate the PET results. The fLuc-4T1 tumor, liver, spleen, and kidneys (i.e. tissues with significant uptake of ^{89}Zr-Df-TRC105-800CW) were also frozen for histological analysis.

Histology

Frozen tissue slices of 5 μm thickness were fixed with cold acetone for 10 min and dried in the air for 30 min. After rinsing with PBS and blocking with 10% donkey serum for 30 min at RT, the slices were incubated with TRC105 (2 μg/mL) for 1 h at 4 °C and visualized using AlexaFluor488-labeled goat anti-human IgG. Tissue slices were also stained for endothelial marker CD31 as described previously.[37, 38] After washing with PBS, the slices were incubated with rat anti-mouse CD31 antibody (2 μg/mL) for 1 h, followed by Cy3-labeled donkey anti-rat IgG for 30 min. All images were acquired with a Nikon Eclipse Ti microscope, under the same condition, and displayed at the same scale. Magnification: 200×.

Radiation Dosimetry Extrapolation to Human

Estimated human dosimetry was calculated from serial PET imaging results on BALB/c female mice injected with ^{89}Zr-Df-TRC105-800CW. ROI analysis was carried out on major organs and time-activity curves were generated from the mean values obtained in mice for each organ of interest. Source organ residence times were then calculated for the human model by integrating a mono-exponential fit to the experimental biodistribution data for major organs (e.g. heart, lung, liver, and kidneys) and the whole body. The source organ residence times obtained forthwith were used with a standard quantitation platform Organ Level Internal Dose Assessment.[39]

Statistical Analysis

Quantitative data were expressed as mean ± SD. Means were compared using Student's t-test. P values < 0.05 were considered statistically significant.

RESULTS

Synthesis and Characterization of the PET/NIRF Probe

On average there is about 1 Df and 0.9 800CW per TRC105 or cetuximab molecule based on UV measurement, which not only minimized potential interference with their biological function but also avoided self-quenching of 800CW, which would occur through fluorescence resonance energy transfer if more than one 800CW molecules are conjugated to the same mAb. Conjugation of both Df and 800CW to TRC105 did not alter the CD105 binding affinity, as evidenced by flow cytometry analysis (Figure 2A). In HUVECs which express a high level of CD105 ($> 10^6$ per cell),[40, 41] there was no observable difference between TRC105 and Df-TRC105-800CW at two non-antigen-saturating concentrations of 1 μg/mL or 5 μg/mL. The binding to HUVECs was CD105-specific, as neither TRC105 nor Df-TRC105-800CW bound to CD105-negative MCF-7 human breast cancer cells,[41] even at a much higher concentration of 10 μg/mL.

^{89}Zr-labeling including final purification using PD-10 columns took 100 ± 10 min (n = 10). The decay-corrected radiochemical yield was 55 ± 14 %, based on 0.25 mg of protein (Df-TRC105-800CW or Df-cetuximab-800CW) per 37 MBq of ^{89}Zr, with specific activity of both ^{89}Zr-Df-TRC105-800CW and ^{89}Zr-Df-cetuximab-800CW being about 80 MBq/mg protein (i.e. 12 GBq/μmol). There was no observable difference between TRC105 and cetuximab during Df/800CW conjugation or ^{89}Zr-labeling.

BLI to Monitor Lung Metastasis

Stable transfection of 4T1 murine breast cancer cells with firefly luciferase did not cause any observable changes in cell proliferation, tumorigenicity, or migration.[32] About one week after i.v. injection, BLI signal of the fLuc-4T1 cells in mouse lung was readily detected after i.p. injection of D-luciferin (Figure 2B&C). At around three weeks after tumor inoculation, when the BLI signal was sufficiently strong but before mice showed observable symptoms (e.g. body weight loss, difficulty in breathing, etc.), mice bearing fLuc-4T1 lung metastasis tumors were used for subsequent PET/NIRF imaging studies. The use of BLI enabled convenient and non-invasive monitoring of the tumor burden in the mice lungs, which ensured that only mice with appropriate tumor burden were used for dual-modality PET/NIRF imaging of tumor angiogenesis, since small microscopic tumors may not have sufficient angiogenic activity for imaging applications.

In Vivo Imaging and Quantitative Data Analysis

The time points of 4, 24, and 48 h p.i. were chosen for serial PET scans after i.v. tracer injection, where the first time point was during initial tumor accumulation phase and tumor uptake at the other two time points were in a plateau. Coronal slices that contain the fLuc-4T1 lung metastasis tumors are shown in Figure 3A and representative PET/CT fused images at 48 h p.i. are shown in Figure 3B&C. At the early time point of 4 h p.i., radioactivity in the blood was prominent. Significant uptake of ^{89}Zr-Df-TRC105-800CW in the lung metastasis tumors was observed at 24 h p.i. with PET, which became more clearly delineated at 48 h p.i. with multiple tumor nodules visible in the lung. Tumor nodules in the mice lung were confirmed with PET/CT fused images (Figure 3B&C).

Tracer uptake in the fLuc-4T1 lung metastasis tumors was much lower in both control groups, where mice were injected with ^{89}Zr-Df-cetuximab-800CW or injected with a blocking dose (2 mg) of TRC105 several hours before ^{89}Zr-Df-TRC105-800CW administration (Figure 3A&B), which strongly suggested CD105 specificity of ^{89}Zr-Df-TRC105-800CW in vivo. Since cetuximab does not cross-react with murine tissues, ^{89}Zr-Df-cetuximab-800CW served as an excellent isotype-matched control for investigating tracer uptake in the fLuc-4T1 lung metastasis tumor solely based on the enhanced permeability and retention effect. There was also significant tracer uptake in the liver, which is mainly due to hepatic clearance similar to other radiolabeled antibodies.[34, 42–44] Since the lung metastasis tumors are deep in the mouse body, in vivo NIRF imaging was not able to delineate the tumor non-invasively, due to limited tissue penetration of light even in the NIR window. Thus, ex vivo NIRF imaging was performed to validate the PET results, as described later in the text.

Quantitative data obtained from ROI analysis of the PET data are shown in Figure 4. For ^{89}Zr-Df-TRC105-800CW, blood pool activity was prominent at early time points, due to long circulation half-life of TRC105, which gradually declined over time (14.7 ± 1.5, 7.9 ± 0.6, and 7.4 ± 1.1 %ID/g at 4, 24, and 48 h p.i. respectively; n = 4; Figure 4A). Liver uptake was 18.3 ± 1.7, 16.8 ± 2.2, and 16.2 ± 2.2 %ID/g at 4, 24, and 48 h p.i. respectively (n = 4). Importantly, uptake of ^{89}Zr-Df-TRC105-800CW in the fLuc-4T1 lung metastasis tumors was prominent even at early time points, which remained stable over time (8.7 ± 1.4, 10.9 ± 0.5, and 9.7 ± 1.1 %ID/g at 4, 24, and 48 h p.i. respectively; n = 4).

Administration of a blocking dose of TRC105 before ^{89}Zr-Df-TRC105-800CW injection significantly reduced tracer uptake in the fLuc-4T1 tumor (4.2 ± 0.4, 4.9 ± 0.5, and 4.9 ± 0.3 %ID/g at 4, 24, and 48 h p.i. respectively; n = 4; $P < 0.01$ at all three time points when compared with mice injected with ^{89}Zr-Df-TRC105-800CW alone; Figure 4B&D). Tracer uptake in the normal organs was not substantially different after blocking, including the liver (19.5 ± 2.7, 17.8 ± 1.2, and 17.5 ± 0.7 %ID/g at 4, 24, and 48 h p.i. respectively; n = 4). These findings suggested that pre-injection of TRC105 saturated available CD105 in the mice (mostly in the fLuc-4T1 lung metastasis tumors but not expressed at a high level in normal organs), which resulted in significantly reduced tumor uptake and confirmed CD105 specificity of the tracer in vivo.

Based on the enhanced permeability and retention effect only, ^{89}Zr-Df-cetuximab-800CW had significantly lower uptake in the fLuc-4T1 lung metastasis tumors (4.3 ± 0.6, 4.2 ± 0.3, and 4.9 ± 0.3 %ID/g at 4, 24, and 48 h p.i. respectively; n = 4; $P < 0.01$; Figure 4C&D) than ^{89}Zr-Df-TRC105-800CW at all three time points, which further confirmed CD105 specificity of ^{89}Zr-Df-TRC105-800CW in the metastatic lesions in vivo.

Ex Vivo Imaging and Biodistribution Studies

After the last PET scans at 48 h p.i., mice were euthanized and major organs were subjected for ex vivo BLI/NIRF/PET imaging (Figure 5A). BLI clearly delineated multiple fLuc-4T1 tumor nodules (about 1 mm in diameter) in the mice lung, which confirmed stable expression of firefly luciferase in the fLuc-4T1 cells and corroborated the in vivo BLI findings. Both ex vivo NIRF and PET imaging findings correlated very well with the in vivo data, in which the fLuc-4T1 lung metastasis tumor uptake of ^{89}Zr-Df-TRC105-800CW was higher than most major organs except the liver. Similar tracer uptake in normal organs was observed for all three groups. However, tumor uptake of ^{89}Zr-Df-cetuximab-800CW and ^{89}Zr-Df-TRC105-800CW of the "blocking" group was significantly lower than that of ^{89}Zr-Df-TRC105-800CW. Of note, PET images represent thin slices of the tissue, while the BLI and NIRF images are both planar projection images. Heterogeneity of the tracer/tumor distribution in the murine lung precludes "perfect match" of images acquired using different modalities. Taken together, ex vivo imaging findings confirmed the in vivo data and further validated CD105 specificity of ^{89}Zr-Df-TRC105-800CW in vivo.

Biodistribution studies after ex vivo BLI/NIRF/PET imaging was also in good agreement with the in vivo PET results, where the fLuc-4T1 lung metastasis tumors had higher uptake of ^{89}Zr-Df-TRC105-800CW than all major organs except the liver (the major organ for clearance of radiolabeled mAbs) (Figure 5B). Spleen and kidneys also had significant uptake of ^{89}Zr-Df-TRC105-800CW at 48 h p.i., however the absolute uptake level was significantly lower than that in the fLuc-4T1 lung metastasis tumors. On average the weight difference between the fLuc-4T1 tumor-bearing lung and normal lung was about 0.1g, which correlates to a total tumor volume of ~100 mm^3. The ratio of ^{89}Zr-Df-TRC105-800CW uptake in the fLuc-4T1 tumor-bearing lung and normal lung was about 3.5:1 based on biodistribution studies at 48 h p.i.

A comparison of the biodistribution data between ^{89}Zr-Df-TRC105-800CW and ^{89}Zr-Df-cetuximab-800CW at 48 h p.i. revealed that the uptake of ^{89}Zr-Df-cetuximab-800CW was similar to ^{89}Zr-Df-TRC105-800CW in most organs except the fLuc-4T1 tumor-bearing lung (Figure 5B). When comparing ^{89}Zr-Df-TRC105-800CW and the "blocking" group, a similar trend was also observed: comparable tracer uptake in most normal tissues but significantly lower uptake in the fLuc-4T1 tumor-bearing lung in the "blocking" group (Figure 5C). Statistical significance was achieved for the fLuc-4T1 tumor-bearing lung for bother comparisons, ($P < 0.01$; $n = 4$), corroborating the PET findings. At 48 h p.i., excellent image contrast with a tumor/muscle ratio of 11.9 ± 1.3 ($n = 4$) was achieved for ^{89}Zr-Df-TRC105-800CW. Overall, the quantification results obtained from biodistribution studies and PET scans matched very well, confirming that quantitative ROI analysis of non-invasive PET scans truly reflected tracer distribution in vivo.

Histology and Radiation Dosimetry

Immunofluorescence CD105/CD31 co-staining of various tissues revealed that CD105 expression in the fLuc-4T1 lung metastasis tumors was primarily on the tumor vasculature, as evidenced by excellent co-localization of CD105 and CD31 staining (Figure 6), and CD105 expression in the fLuc-4T1 tumor-bearing lung was much higher than that in the normal lung. Mouse liver and spleen both exhibited very low level of CD105 staining, indicating that these tissues do not have significant level of CD105 expression. Therefore, uptake of ^{89}Zr-Df-TRC105-800CW in the liver/spleen was largely unrelated to CD105 binding, but more related to non-specific capture by the reticuloendothelial system and hepatic clearance of the tracer. Uptake of ^{89}Zr-Df-TRC105-800CW was noted in the kidneys, which reflected CD105 expression (mostly in the renal medulla). However, since mAbs do not undergo renal clearance and the superb stability of ^{89}Zr-Df complex prevents

significant amount of ^{89}Zr-containing low-molecular weight species,[34, 43] the absolute uptake of ^{89}Zr-Df-TRC105-800CW in the kidney was quite low (~5%ID/g).

Human absorbed doses to normal organs from ^{89}Zr-Df-TRC105-800CW were estimated from serial PET imaging data in BALB/c mice and presented in Table 1. Besides the blood, liver, and lungs, most organs exhibited low level of tracer uptake at all time points examined. There was no significant kidney uptake or renal excretion of the tracer due to its high molecular weight (~150 kDa). These results predicted that the highest radiation-absorbed doses will be to the heart wall (0.83 ± 0.09 mSv/MBq) and liver (0.44 ± 0.04 mSv/MBq). The whole-body absorbed dose was found to be 0.042 ± 0.003 mSv/MBq. Although the radiation doses to the heart, liver, and lungs are higher than other radiolabeled mAbs reported in the literature,[37, 45, 46] the doses to other major organs (e.g. kidneys, spleen, etc.) are much lower.

DISCUSSION

The major goal of this study was to develop a CD105-specific agent for both PET and NIRF imaging of breast cancer lung metastasis. Since the currently accepted standard method for quantifying tumor angiogenesis is CD105-positive microvessel density (MVD; an independent prognostic factor in multiple solid tumor types[7, 8]) through histologic analysis of biopsied/resected tumor tissue, non-invasive whole body measurement of CD105-positive MVD with PET has tremendous clinical potential in early tumor detection, anti-angiogenic drug development, patient stratification, and ultimately in the day-to-day management of cancer patients. Dual-modality PET/NIRF imaging of tumor angiogenesis with a single agent can not only provide complementary information through the two imaging techniques, but also have potential applications in many clinical scenarios including early detection of small metastatic lesions and imaged-guided surgery in breast cancer.

We have achieved our goal in this study. Various in vitro, in vivo, and ex vivo experiments confirmed that ^{89}Zr-Df-TRC105-800CW is CD105 specific, with no observable deterioration in affinity or specificity. The possibility of Df or 800CW conjugation (on average about 1 of each was attached to each TRC105 molecule) at the lysine residue involved in CD105 binding was extremely low, since there is only one lysine residue in each of the CD105-binding regions of TRC105 (which has a total of ~1400 amino acid residues).[8] The tumor nodules in the fLuc-4T1 lung are generally 1–2 mm in diameter, indicating that ^{89}Zr-Df-TRC105-800CW can be used for early detection of small metastatic lesions. Of note, the imaging target (i.e. CD105) is overexpressed during tumor angiogenesis which does not become significant until tumors are about 1 mm in diameter. Furthermore, detection of lesions smaller than 1 mm is more limited by the spatial resolution of the PET scanners available (~1.5 mm for small animal PET and ~4 mm for clinical PET), rather than the imaging agent itself.

Due to limited tissue penetration of fluorescence signal and deep tissue nature of the fLuc-4T1 lung metastasis tumors, in vivo NIRF imaging did not clearly delineate tumors in the lung. Ex vivo NIRF imaging was therefore performed to validate PET imaging findings. Although NIRF imaging is not as quantitative as PET (or biodistribution) studies, we did analyze the linear correlation between the two imaging techniques. In this regard, a total of 24 data points (tumor and liver uptake for 3 groups of mice with 4 mice per group) were used to evaluate the linear correlation between the fluorescence signal intensity (obtained from ROI analysis of the ex vivo NIRF data) and the %ID/g values (obtained from ROI analysis of the in vivo PET data). The rationale for only using the data for liver and the fLuc-4T1 tumor was that these are the two tissues/organs with the highest tracer uptake, therefore the quantification data for both PET and NIRF was more accurate than many of the

other organs. A statistically significant (P = 0.0002) linear correlation was observed, with an R value of 0.689. Hence, ex vivo NIRF imaging was able to provide semi-quantitative information about tracer distribution, when tissue absorption and autofluorescence was reduced to a minimum (e.g. ex vivo imaging of harvested organs).

With regard to image-guided surgery, the metastatic tumor nodules are in the murine lung which is challenging to operate while keeping the mice alive. Therefore, comprehensive ex vivo imaging studies were performed to examine/mimic this aspect. In addition, we have investigated tumor removal with surgical guidance in subcutaneous 4T1 tumor models to further demonstrate the utility of this dual-modality agent, where NIRF imaging was employed to confirm complete removal of the tumor (Figure 7). Since the BALB/c mice used in this study has white hair which can affect NIRF imaging to a certain extent (e.g. light absorption, scattering, etc.), we have also inoculated 4T1 tumor cells in nude mice and performed image-guided surgery, which did give significantly “cleaner” images.

Mouse models of cancer have become indispensable in the discovery and assessment of new imaging/therapeutic agents in biomedical research.[47] After demonstrating the proof-of-principle for non-invasive imaging of CD105 expression on the tumor vasculature in a subcutaneous 4T1 tumor model,[34, 36, 48] herein we investigated a dual-labeled agent for both PET and NIRF imaging of CD105 in a breast cancer experimental lung metastasis model that is more relevant to the biological processes occurring during tumor progression. Metastasis is a malignant feature of cancer and a large body of research has revealed that tumor metastasis is a complex and multi-step process.[1, 3] For a tumor cell to metastasize, it must detach from the primary lesion and invade the surrounding tissue, intravasate into the circulatory system, avoid host immune defenses, arrest at a distant site, extravasate, and proliferate. The experimental lung metastasis model used in this study can simulate some of these processes. However, monitoring the tumor growth in experiment lung metastasis model is difficult to achieve using traditional approaches, which usually requires large numbers of animals to be sacrificed at multiple time points to overcome the variability between animals. These facts underscore the importance of using imaging tools to non-invasively monitor the tumor burden in vivo, such as longitudinal BLI as we employed in this study.

When compared with other antibody-based PET tracers,[37, 43, 46, 49] tumor uptake in this study is relatively low (~10 %ID/g at the peak). This is partly due to the fact that ^{89}Zr-Df-TRC105-800CW targets only the tumor vasculature but not the fLuc-4T1 tumor cells. There are significantly fewer tumor vascular endothelial cells than tumor cells, which are the targets of most antibodies used for cancer imaging. In addition, the tumor nodules in the lung (~1 mm in diameter) are much smaller than the subcutaneous tumors used in most studies (> 5 mm in diameter). Therefore the angiogenic activity in the fLuc-4T1 lung metastasis tumors is lower than subcutaneous 4T1 tumors that are growing exponentially. Since the fLuc-4T1 tumor nodules are quite small, partial volume effect of the PET scanner may cause underestimation of the tumor uptake. Biodistribution studies were carried out on all mice to quantitatively measure tracer uptake in the lung metastasis tumors, which correlated well with the PET data. Furthermore, tumor vasculature in the fLuc-4T1 model is of murine origin, whereas TRC105 has lower affinity to murine CD105 than its human homolog.[50] Although the fLuc-4T1 lung metastasis model is not optimal for testing TRC105, excellent tumor contrast and prominent tumor uptake was nonetheless achieved for mm-sized lesions, suggesting that ^{89}Zr-Df-TRC105-800CW may potentially be used for early detection of small metastatic lesions in breast cancer patients, as well as providing surgical guidance for tumor resection with the NIRF dye. It is possible that this tracer may perform better in cancer patients (who express human CD105 in the tumor vasculature) than in the murine model used here.

^{89}Zr-labeling of mAbs was usually achieved through various types of chelators, with Df been the most widely used.[35, 51] Recently, Df-Bz-NCS was reported as a new bifunctional chelator for ^{89}Zr labeling, which significantly simplified the radiochemistry from the initial 6-step strategy into a 2-step procedure.[52] Df has been safely used in the clinic for many years, with neither adverse reactions nor significant changes in blood and urine values observed after injection of various Df-containing conjugates.[20, 21] In addition, no antibody responses directed against Df were observed, indicating its low immunogenicity.[53]

For future investigation, the following strategies may be adopted to better mimic the clinical situation and further improve the tumor uptake/contrast: using a mAb that binds murine CD105 with high affinity (with the caveat that the imaging agent is less amenable for clinical translation), or carrying out studies in transgenic mice whose vasculature expresses human CD105. Since the dosimetry of ^{89}Zr-based tracers is relatively high, due to the presence of high energy γ emission, other PET isotopes (e.g. ^{64}Cu, ^{44}Sc, ^{90}Nb) should also be investigated. In the recently completed Phase I trial, the terminal half-life of TRC105 was found to be dependent on the injected dose.[11] On an every 2 week schedule, the terminal half-life of TRC105 in patients was 7.4, 10.8, and 42.8 h for 3, 10, and 15 mg/kg doses, respectively. Therefore, for future clinical translation, ^{89}Zr-labeling may be necessary for patients injected with higher doses of TRC105 (> 10 mg/kg). Upon further development and optimization, TRC105-based imaging agents will have broad clinical relevance/applications in a variety of cancer types, since all solid tumors depend on angiogenesis.

CONCLUSION

Herein we report PET/NIRF imaging of CD105 expression using ^{89}Zr-Df-TRC105-800CW, in a mouse model of breast cancer experimental lung metastasis. Broad clinical potential of TRC105-based imaging agents was shown in many solid tumor types, which also enabled non-invasive detection of small metastatic tumor nodules and intraoperative guidance for tumor removal.

Supplementary Material

Refer to Web version on PubMed Central for supplementary material.

Acknowledgments

This work is supported, in part, by the University of Wisconsin Carbone Cancer Center, the Department of Defense (W81XWH-11-1-0644 and W81XWH-11-1-0648), NCRR 1UL1RR025011, and the NIH through the UW Radiological Sciences Training Program 5 T32 CA009206-32. We thank Dr. Jamey P. Weichert and Mohammed Farhoud for their help with the imaging studies.

REFERENCES

1. Mehlen P, Puisieux A. Metastasis: a question of life or death. Nat Rev Cancer. 2006; 6:449–458. [PubMed: 16723991]
2. Siegel R, Ward E, Brawley O, Jemal A. Cancer statistics, 2011: The impact of eliminating socioeconomic and racial disparities on premature cancer deaths. CA Cancer J Clin. 2011; 61:212–236. [PubMed: 21685461]
3. Weigelt B, Peterse JL, van 't Veer LJ. Breast cancer metastasis: markers and models. Nat Rev Cancer. 2005; 5:591–602. [PubMed: 16056258]
4. Hanahan D, Weinberg RA. Hallmarks of cancer: the next generation. Cell. 2011; 144:646–674. [PubMed: 21376230]
5. von Elstermann M. Metastasis: Which way to the lungs? Nat Rev Cancer. 2008; 8:410–411.

6. Ikushima H, Miyazono K. TGFbeta signalling: a complex web in cancer progression. Nat Rev Cancer. 2010; 10:415–424. [PubMed: 20495575]
7. Fonsatti E, Nicolay HJ, Altomonte M, Covre A, Maio M. Targeting cancer vasculature via endoglin/CD105: a novel antibody-based diagnostic and therapeutic strategy in solid tumours. Cardiovasc Res. 2010; 86:12–19. [PubMed: 19812043]
8. Seon BK, Haba A, Matsuno F, Takahashi N, Tsujie M, She X, Harada N, Uneda S, Tsujie T, Toi H, Tsai H, Haruta Y. Endoglin-targeted cancer therapy. Curr Drug Deliv. 2011; 8:135–143. [PubMed: 21034418]
9. Zhang Y, Yang Y, Hong H, Cai W. Multimodality molecular imaging of CD105 (Endoglin) expression. Int J Clin Exp Med. 2011; 4:32–42. [PubMed: 21394284]
10. Dallas NA, Samuel S, Xia L, Fan F, Gray MJ, Lim SJ, Ellis LM. Endoglin (CD105): a marker of tumor vasculature and potential target for therapy. Clin Cancer Res. 2008; 14:1931–1937. [PubMed: 18381930]
11. Mendelson DS, Gordon MS, Rosen LS, Hurwitz H, Wong MK, Adams BJ, Alvarez D, Seon BK, Theuer CP, Leigh BR. Phase I study of TRC105 (anti-CD105 [endoglin] antibody) therapy in patients with advanced refractory cancer. J Clin Oncol. 2010; 28:15s.
12. Gambhir SS, Czernin J, Schwimmer J, Silverman DH, Coleman RE, Phelps ME. A tabulated summary of the FDG PET literature. J Nucl Med. 2001; 42:1S–93S. [PubMed: 11483694]
13. Alauddin MM. Positron emission tomography (PET) imaging with ^{18}F-based radiotracers. Am J Nucl Med Mol Imaging. 2012; 2:55–76. [PubMed: 23133802]
14. Eary JF, Hawkins DS, Rodler ET, Conrad EU. I. ^{18}F-FDG PET in sarcoma treatment response imaging. Am J Nucl Med Mol Imaging. 2011; 1:47–53. [PubMed: 23133794]
15. Grassi I, Nanni C, Allegri V, Morigi JJ, Montini GC, Castellucci P, Fanti S. The clinical use of PET with ^{11}C-acetate. Am J Nucl Med Mol Imaging. 2012; 2:33–47. [PubMed: 23133801]
16. Iagaru A. ^{18}F-FDG PET/CT: timing for evaluation of response to therapy remains a clinical challenge. Am J Nucl Med Mol Imaging. 2011; 1:63–64. [PubMed: 23133796]
17. Koo V, Hamilton PW, Williamson K. Non-invasive in vivo imaging in small animal research. Cell Oncol. 2006; 28:127–139. [PubMed: 16988468]
18. Pomper MG, Lee JS. Small animal imaging in drug development. Curr Pharm Des. 2005; 11:3247–3272. [PubMed: 16250853]
19. Wu AM. Antibodies and antimatter: the resurgence of immuno-PET. J Nucl Med. 2009; 50:2–5. [PubMed: 19091888]
20. van Dongen GA, Vosjan MJ. Immuno-positron emission tomography: shedding light on clinical antibody therapy. Cancer Biother Radiopharm. 2010; 25:375–385. [PubMed: 20707716]
21. Zhang Y, Hong H, Cai W. PET tracers based on Zirconium-89. Curr Radiopharm. 2011; 4:131–139. [PubMed: 22191652]
22. van Dam GM, Themelis G, Crane LM, Harlaar NJ, Pleijhuis RG, Kelder W, Sarantopoulos A, de Jong JS, Arts HJ, van der Zee AG, Bart J, Low PS, Ntziachristos V. Intraoperative tumor-specific fluorescence imaging in ovarian cancer by folate receptor-alpha targeting: first in-human results. Nat Med. 2011; 17:1315–1319. [PubMed: 21926976]
23. Chin PTK, Beekman CAC, Buckle T, Josephson L, van Leeuwen FWB. Multispectral visualization of surgical safety-margins using fluorescent marker seeds. Am J Nucl Med Mol Imaging. 2012; 2:151–162. [PubMed: 23133810]
24. Zhang Y, Hong H, Engle JW, Yang Y, Barnhart TE, Cai W. Positron emission tomography and near-infrared fluorescence imaging of vascular endothelial growth factor with dual-labeled bevacizumab. Am J Nucl Med Mol Imaging. 2012; 2:1–13. [PubMed: 22229128]
25. Cai W, Hsu AR, Li ZB, Chen X. Are quantum dots ready for *in vivo* imaging in human subjects? Nanoscale Res Lett. 2007; 2:265–281. [PubMed: 21394238]
26. Cai W, Hong H. In a “nutshell”: intrinsically radio-labeled quantum dots. Am J Nucl Med Mol Imaging. 2012; 2:136–140. [PubMed: 23133808]
27. Huang X, Lee S, Chen X. Design of “smart” probes for optical imaging of apoptosis. Am J Nucl Med Mol Imaging. 2011; 1:3–17. [PubMed: 22514789]

28. Cai W, Chen K, Li ZB, Gambhir SS, Chen X. Dual-function probe for PET and near-infrared fluorescence imaging of tumor vasculature. J Nucl Med. 2007; 48:1862–1870. [PubMed: 17942800]
29. Sampath L, Kwon S, Hall MA, Price RE, Sevick-Muraca EM. Detection of Cancer Metastases with a Dual-labeled Near-Infrared/Positron Emission Tomography Imaging Agent. Transl Oncol. 2010; 3:307–217. [PubMed: 20885893]
30. Zhang Y, Hong H, Engle JW, Yang Y, Theuer CP, Barnhart TE, Cai W. Positron Emission Tomography and Optical Imaging of Tumor CD105 Expression with a Dual-Labeled Monoclonal Antibody. Mol Pharm. 2012; 9:645–653. [PubMed: 22292418]
31. Cai W, Niu G, Chen X. Multimodality imaging of the HER-kinase axis in cancer. Eur J Nucl Med Mol Imaging. 2008; 35:186–208. [PubMed: 17846765]
32. Cao Q, Cai W, Niu G, He L, Chen X. Multimodality imaging of IL-18-binding protein-Fc therapy of experimental lung metastasis. Clin Cancer Res. 2008; 14:6137–6145. [PubMed: 18829492]
33. Holland JP, Sheh Y, Lewis JS. Standardized methods for the production of high specific-activity zirconium-89. Nucl Med Biol. 2009; 36:729–739. [PubMed: 19720285]
34. Hong H, Severin GW, Yang Y, Engle JW, Zhang Y, Barnhart TE, Liu G, Leigh BR, Nickles RJ, Cai W. Positron emission tomography imaging of CD105 expression with ^{89}Zr-Df-TRC105. Eur J Nucl Med Mol Imaging. 2012; 39:138–148. [PubMed: 21909753]
35. Vosjan MJ, Perk LR, Visser GW, Budde M, Jurek P, Kiefer GE, van Dongen GA. Conjugation and radiolabeling of monoclonal antibodies with zirconium-89 for PET imaging using the bifunctional chelate p-isothiocyanatobenzyl-desferrioxamine. Nat Protoc. 2010; 5:739–743. [PubMed: 20360768]
36. Yang Y, Zhang Y, Hong H, Liu G, Leigh BR, Cai W. In vivo near-infrared fluorescence imaging of CD105 expression. Eur J Nucl Med Mol Imaging. 2011; 38:2066–2076. [PubMed: 21814852]
37. Cai W, Wu Y, Chen K, Cao Q, Tice DA, Chen X. *In vitro* and *in vivo* characterization of ^{64}Cu-labeled Abegrin™, a humanized monoclonal antibody against integrin $\alpha_v\beta_3$. Cancer Res. 2006; 66:9673–9681. [PubMed: 17018625]
38. Cai W, Chen K, Mohamedali KA, Cao Q, Gambhir SS, Rosenblum MG, Chen X. PET of vascular endothelial growth factor receptor expression. J Nucl Med. 2006; 47:2048–2056. [PubMed: 17138749]
39. Sgouros G. Dosimetry of internal emitters. J Nucl Med. 2005; 46(Suppl 1):18S–27S. [PubMed: 15653648]
40. Takahashi N, Haba A, Matsuno F, Seon BK. Antiangiogenic therapy of established tumors in human skin/severe combined immunodeficiency mouse chimeras by anti-endoglin (CD105) monoclonal antibodies, and synergy between anti-endoglin antibody and cyclophosphamide. Cancer Res. 2001; 61:7846–7854. [PubMed: 11691802]
41. Fonsatti E, Jekunen AP, Kairemo KJ, Coral S, Snellman M, Nicotra MR, Natali PG, Altomonte M, Maio M. Endoglin is a suitable target for efficient imaging of solid tumors: *in vivo* evidence in a canine mammary carcinoma model. Clin Cancer Res. 2000; 6:2037–2043. [PubMed: 10815930]
42. Dijkers EC, Oude Munnink TH, Kosterink JG, Brouwers AH, Jager PL, de Jong JR, van Dongen GA, Schroder CP, Lub-de Hooge MN, de Vries EG. Biodistribution of ^{89}Zr-trastuzumab and PET imaging of HER2-positive lesions in patients with metastatic breast cancer. Clin Pharmacol Ther. 2010; 87:586–592. [PubMed: 20357763]
43. Holland JP, Divilov V, Bander NH, Smith-Jones PM, Larson SM, Lewis JS. ^{89}Zr-DFO-J591 for immunoPET of prostate-specific membrane antigen expression in vivo. J Nucl Med. 2010; 51:1293–1300. [PubMed: 20660376]
44. Nagengast WB, de Korte MA, Oude Munnink TH, Timmer-Bosscha H, den Dunnen WF, Hollema H, de Jong JR, Jensen MR, Quadt C, Garcia-Echeverria C, van Dongen GA, Lub-de Hooge MN, Schroder CP, de Vries EG. ^{89}Zr-bevacizumab PET of early antiangiogenic tumor response to treatment with HSP90 inhibitor NVP-AUY922. J Nucl Med. 2010; 51:761–767. [PubMed: 20395337]
45. Cutler PD, Schwarz SW, Anderson CJ, Connett JM, Welch MJ, Philpott GW, Siegel BA. Dosimetry of copper-64-labeled monoclonal antibody 1A3 as determined by PET imaging of the torso. J Nucl Med. 1995; 36:2363–2371. [PubMed: 8523133]

46. Cai W, Ebrahimnejad A, Chen K, Cao Q, Li ZB, Tice DA, Chen X. Quantitative radioimmunoPET imaging of EphA2 in tumor-bearing mice. Eur J Nucl Med Mol Imaging. 2007; 34:2024–2036. [PubMed: 17673999]
47. Frese KK, Tuveson DA. Maximizing mouse cancer models. Nat Rev Cancer. 2007; 7:645–658. [PubMed: 17687385]
48. Hong H, Yang Y, Zhang Y, Engle JW, Barnhart TE, Nickles RJ, Leigh BR, Cai W. Positron emission tomography imaging of CD105 expression during tumor angiogenesis. Eur J Nucl Med Mol Imaging. 2011; 38:1335–1343. [PubMed: 21373764]
49. Heskamp S, van Laarhoven HW, Molkenboer-Kuenen JD, Franssen GM, Versleijen-Jonkers YM, Oyen WJ, van der Graaf WT, Boerman OC. ImmunoSPECT and immunoPET of IGF-1R expression with the radiolabeled antibody R1507 in a triple-negative breast cancer model. J Nucl Med. 2010; 51:1565–1572. [PubMed: 20847162]
50. Matsuno F, Haruta Y, Kondo M, Tsai H, Barcos M, Seon BK. Induction of lasting complete regression of preformed distinct solid tumors by targeting the tumor vasculature using two new anti-endoglin monoclonal antibodies. Clin Cancer Res. 1999; 5:371–382. [PubMed: 10037187]
51. Meijs WE, Herscheid JDM, Haisma HJ, Pinedo HM. Evaluation of desferal as a bifunctional chelating agent for labeling antibodies with Zr-89. Int J Radiat Appl Instrum, A, Appl Radiat Isot. 1992; 43:1443–1447.
52. Perk LR, Vosjan MJ, Visser GW, Budde M, Jurek P, Kiefer GE, van Dongen GA. p-Isothiocyanatobenzyl-desferrioxamine: a new bifunctional chelate for facile radiolabeling of monoclonal antibodies with zirconium-89 for immuno-PET imaging. Eur J Nucl Med Mol Imaging. 2010; 37:250–259. [PubMed: 19763566]
53. Borjesson PK, Jauw YW, Boellaard R, de Bree R, Comans EF, Roos JC, Castelijns JA, Vosjan MJ, Kummer JA, Leemans CR, Lammertsma AA, van Dongen GA. Performance of immuno-positron emission tomography with zirconium-89-labeled chimeric monoclonal antibody U36 in the detection of lymph node metastases in head and neck cancer patients. Clin Cancer Res. 2006; 12:2133–2140. [PubMed: 16609026]

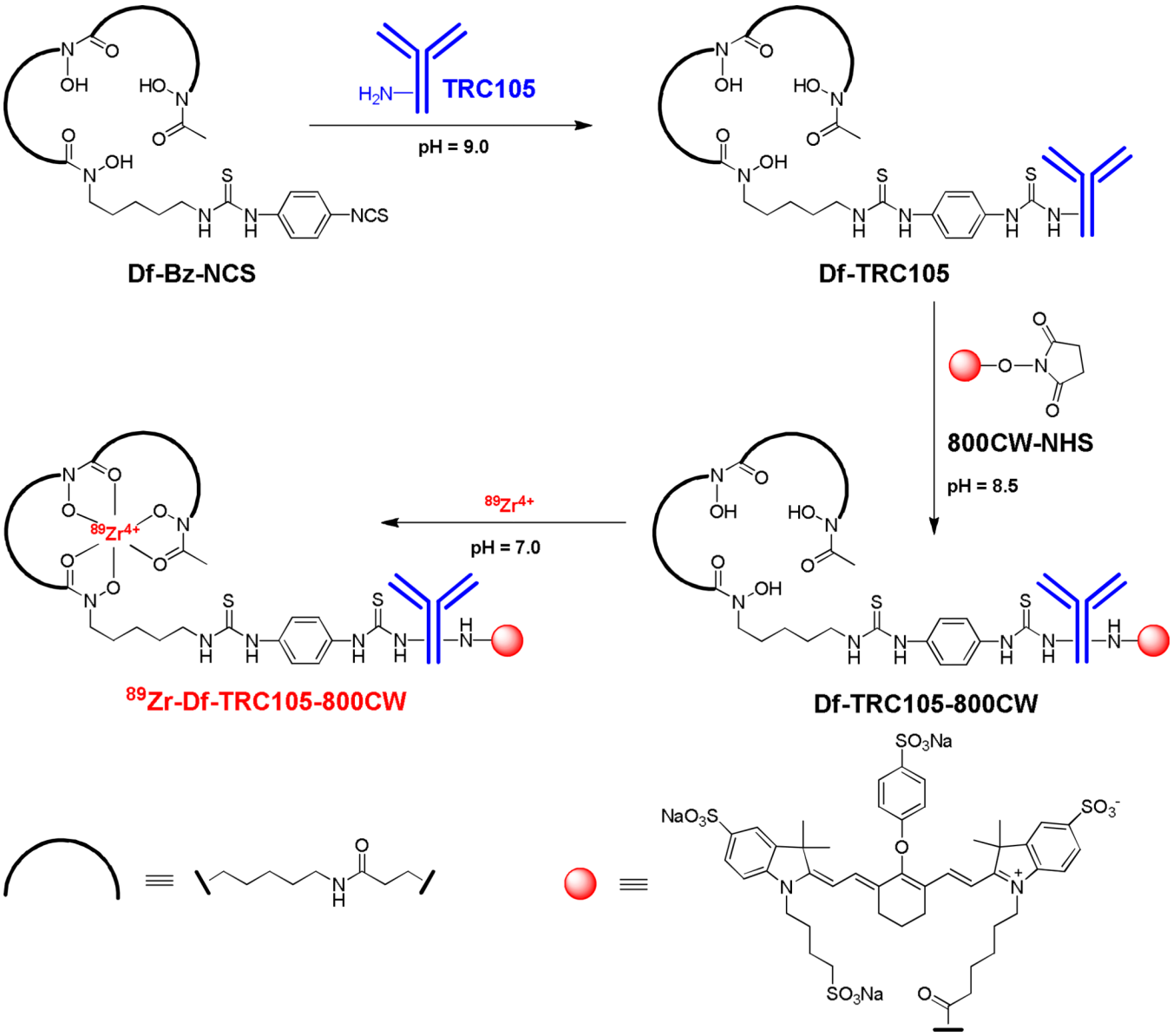

Figure 1.
Synthesis of ^{89}Zr-Df-TRC105-800CW. ^{89}Zr-Df-cetuximab-800CW was prepared in a similar manner.

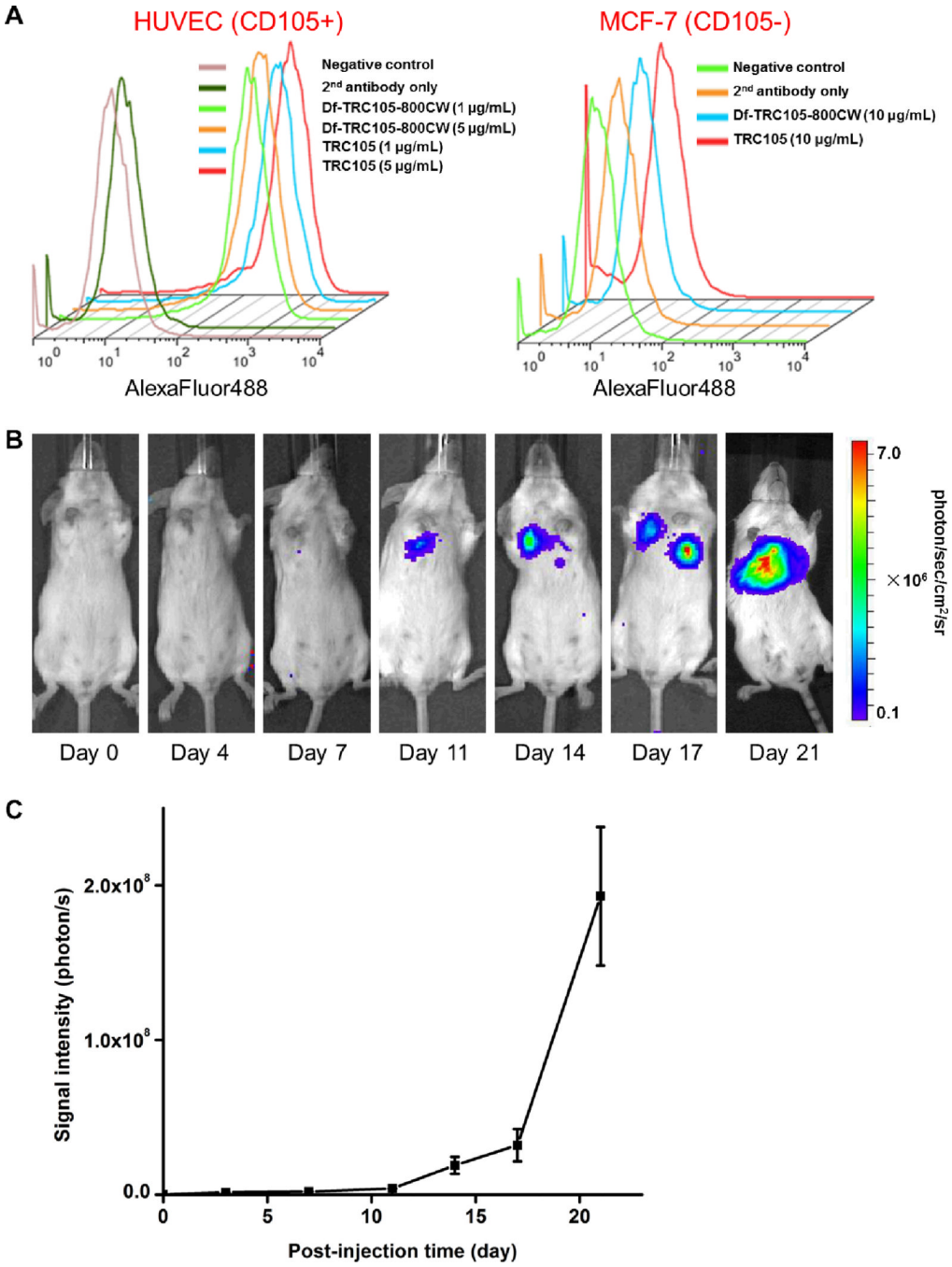

Figure 2.

Characterization of Df-TRC105-800CW and the tumor model. **A.** Flow cytometry analysis of TRC105 and Df-TRC105-800CW in HUVECs (CD105-positive) and MCF-7 human breast cancer cells (CD105-negative) at different concentrations. Data from various control experiments are also shown. **B.** Serial bioluminescence images of tumor-bearing mice after intravenous injection of fLuc-4T1 cells. **C.** Total photon flux of the bioluminescence signal from the lung (n = 8).

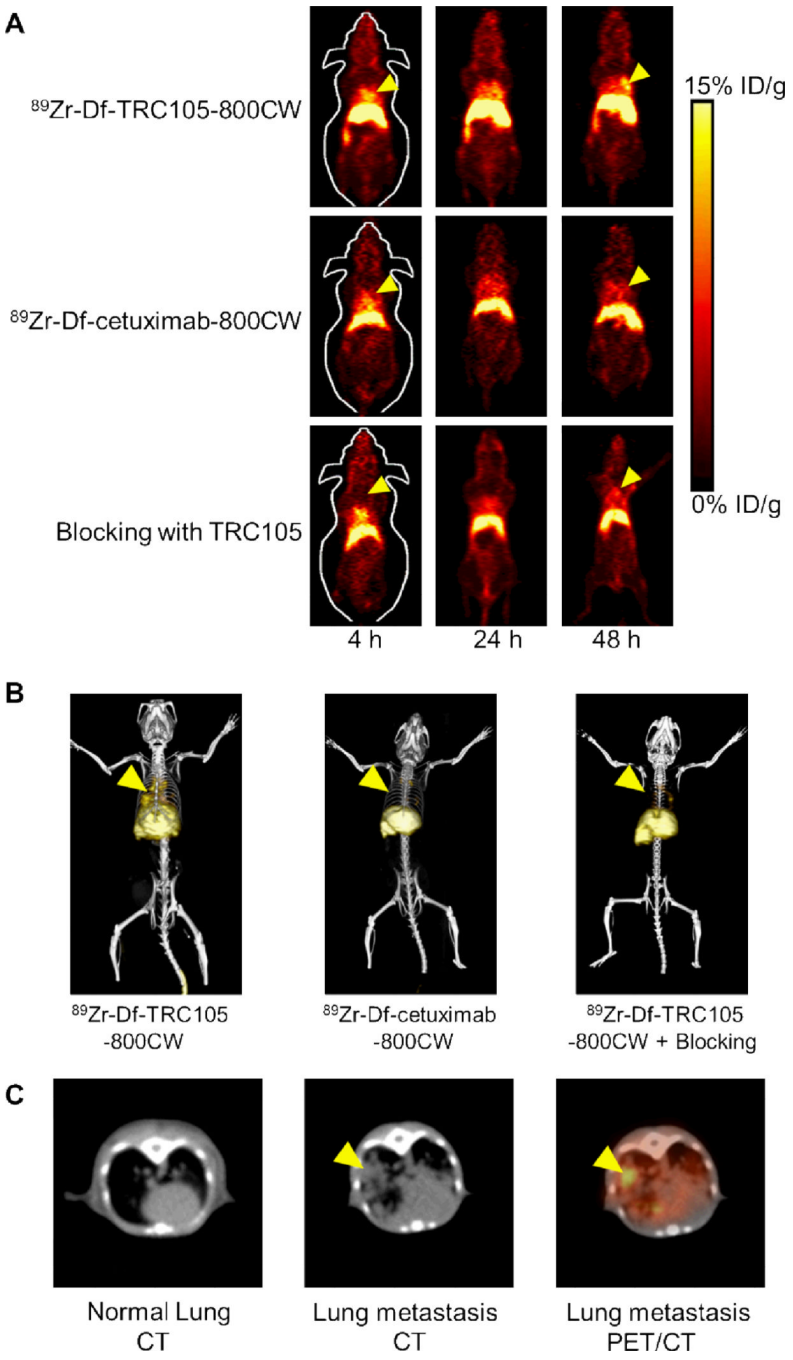

Figure 3.

Serial in vivo PET/CT imaging of fLuc-4T1 tumor-bearing mice. **A.** Serial coronal PET images at 4, 24, and 48 h post-injection of ^{89}Zr-Df-TRC105-800CW, ^{89}Zr-Df-cetuximab-800CW, or ^{89}Zr-Df-TRC105-800CW after a 2 mg dose of TRC105 (i.e. blocking). **B.** Representative PET/CT images of fLuc-4T1 tumor-bearing mouse at 48 h post-injection of ^{89}Zr-Df-TRC105-800CW, ^{89}Zr-Df-cetuximab-800CW, or ^{89}Zr-Df-TRC105-800CW after a 2mg dose of TRC105 (i.e. blocking). **C.** Representative CT images of normal lung, fLuc-4T1 lung metastasis, and a PET/CT fused image at 48 h post-injection of ^{89}Zr-Df-TRC105-800CW. Arrowheads indicate the fLuc-4T1 tumors.

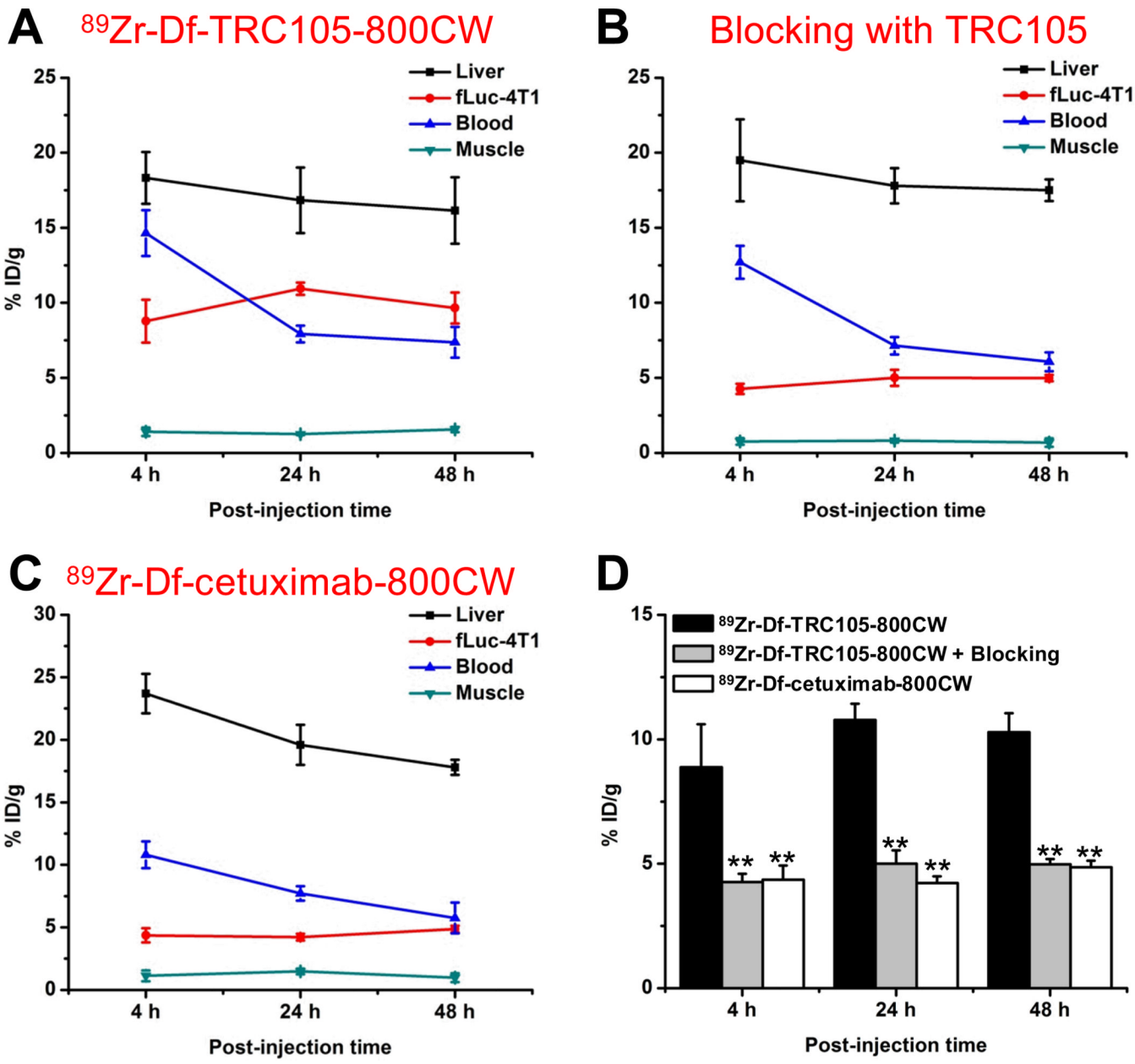

Figure 4.

Quantitative analysis of the PET data. **A.** Time-activity curves of the liver, fLuc-4T1 tumor, blood, and muscle upon intravenous injection of ^{89}Zr-Df-TRC105-800CW. **B.** Time-activity curves of the liver, fLuc-4T1 tumor, blood, and muscle upon intravenous injection of ^{89}Zr-Df-TRC105-800CW, after a blocking dose of TRC105. **C.** Time-activity curves of the liver, fLuc-4T1 tumor, blood, and muscle upon intravenous injection of ^{89}Zr-Df-cetuximab-800CW. **D.** Comparison of the fLuc-4T1 tumor uptake in the three groups. n = 4; **: $P < 0.01$.

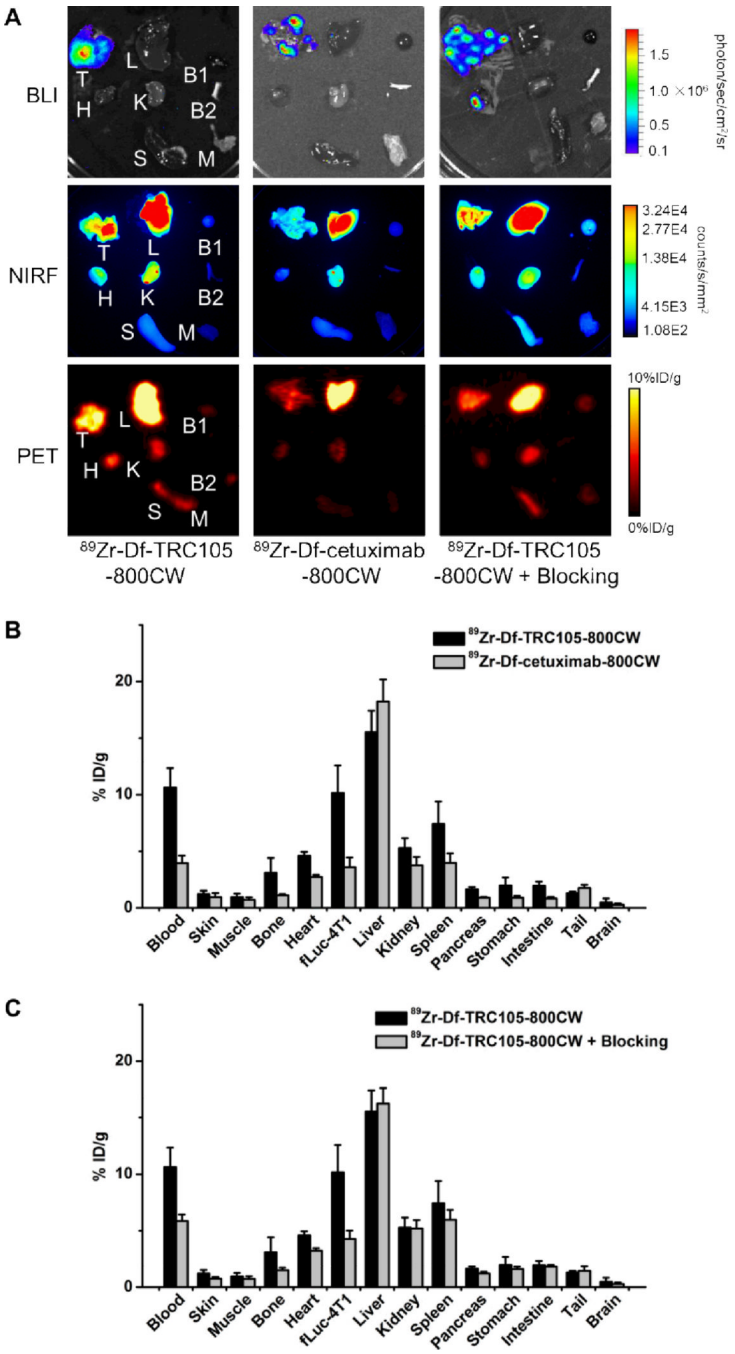

Figure 5.

Ex vivo imaging and biodistribution studies. **A.** Ex vivo bioluminescence imaging (BLI), near-infrared fluorescence (NIRF), and positron emission tomography (PET) imaging of major organs at 48 h post-injection of each tracer. Images are representative of 4 mice per group. T: fLuc-4T1 tumor-bearing lung, L: liver, B1: blood, H: heart, K: kidney, B2: bone, S: spleen, M: muscle. **B.** Biodistribution of ^{89}Zr-Df-TRC105-800CW or ^{89}Zr-Df-cetuximab-800CW in fLuc-4T1 tumor-bearing mice at 48 h post-injection. **C.** Biodistribution in fLuc-4T1 tumor-bearing mice at 48 h post-injection of ^{89}Zr-Df-TRC105-800CW or ^{89}Zr-Df-TRC105-800CW after a blocking dose of TRC105. n = 4.

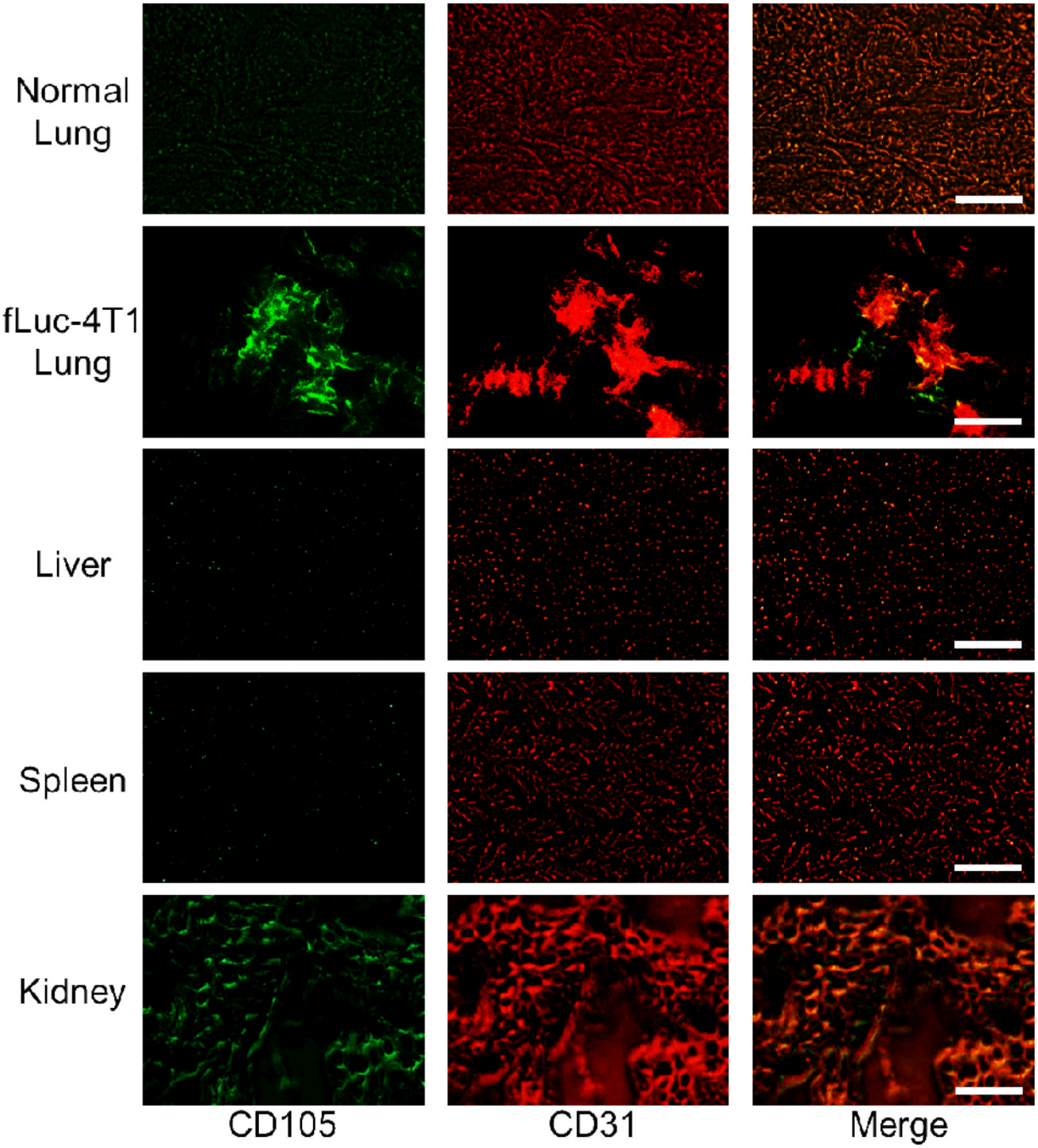

Figure 6.
Immunofluorescence CD105/CD31 double-staining of normal mouse lung, fLuc-4T1 tumor-bearing lung, liver, spleen, and kidney tissue sections. TRC105 and AlexaFluor488-labeled goat anti-human IgG were used for CD105 staining (green). Afterwards, the tissue slices were stained with rat anti-mouse CD31 antibody and Cy3-labeled donkey anti-rat IgG (red). Magnification: 200×. Scale bar: 50 μm.

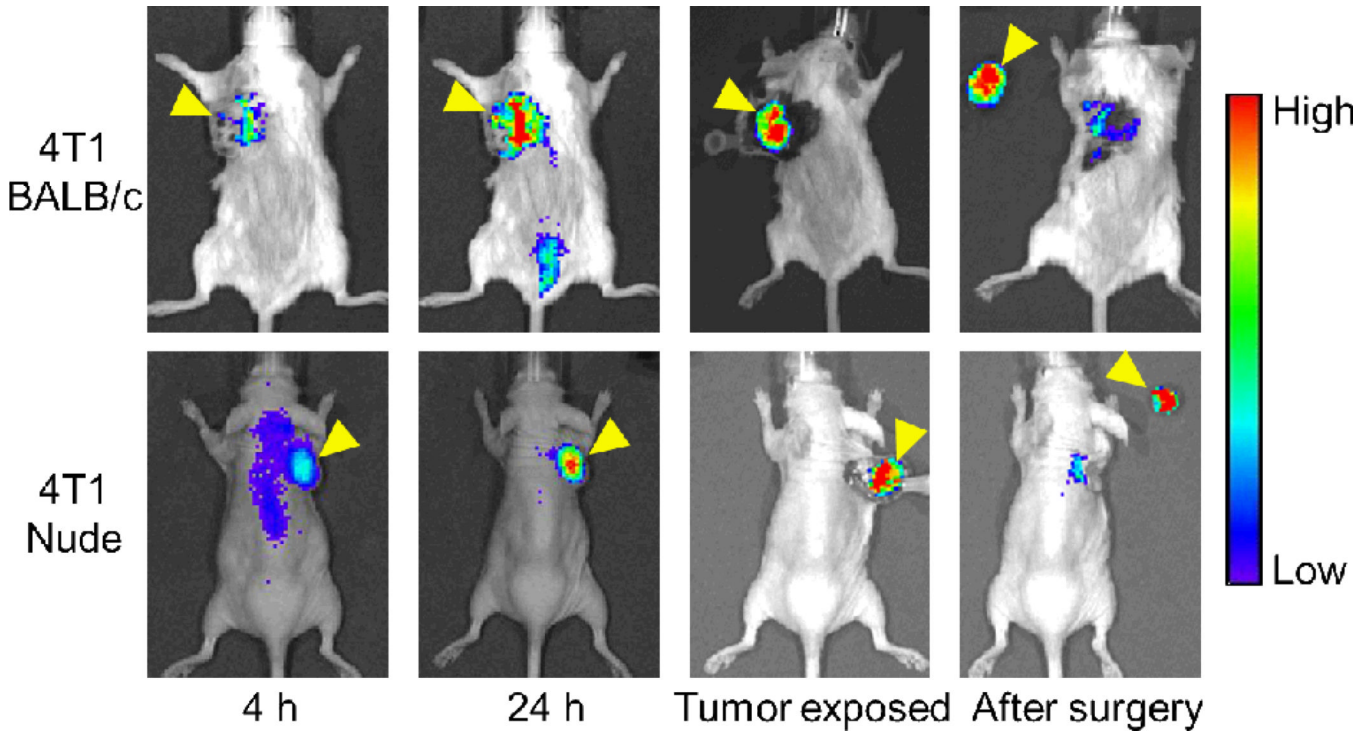

Figure 7.
Near-infrared fluorescence imaging-guided removal of tumors with Df-TRC105-800CW in subcutaneous 4T1 tumor models. Mice were subjected to optical imaging at 4 and 24 h post-injection of Df-TRC105-800CW, immediately after the skin was open and tumor exposed, and after surgical removal of the tumor. Top: BALB/c mice. Bottom: Nude mice. With image guidance, tumor removal was straightforward. The residual fluorescence signal from the original tumor site was due to blood concentration of Df-TRC105-800CW instead of residual tumor tissue. Arrowheads indicate the 4T1 tumors in all cases.

Table 1

Estimated radiation absorbed doses to an adult female after intravenous injection of ^{89}Zr-Df-TRC105-800CW (n = 4).

Target Organ	Total (mSv/MBq)	SD (mSv/MBq)	Total (rem/mCi)	SD (rem/mCi)
Adrenals	9.53E−02	7.17E−03	3.52E−01	2.67E−02
Brain	2.08E−03	2.45E−04	7.68E−03	9.13E−04
Breasts	5.97E−02	5.48E−03	2.21E−01	2.05E−02
Gallbladder Wall	1.26E−01	1.09E−02	4.65E−01	4.11E−02
LLI Wall	8.10E−03	8.79E−04	3.00E−02	3.25E−03
Small Intestine	2.34E−02	1.83E−03	8.67E−02	6.85E−03
Stomach Wall	5.59E−02	4.46E−03	2.07E−01	1.66E−02
ULI Wall	3.28E−02	2.64E−03	1.21E−01	1.00E−02
Heart Wall	8.34E−01	8.78E−02	3.09E+00	3.26E−01
Kidneys	5.24E−02	4.12E−03	1.94E−01	1.52E−02
Liver	4.40E−01	4.21E−02	1.63E+00	1.54E−01
Lungs	1.07E−01	9.31E−03	3.97E−01	3.43E−02
Muscle	3.12E−02	2.94E−03	1.15E−01	1.09E−02
Ovaries	1.18E−02	1.11E−03	4.36E−02	4.07E−03
Pancreas	9.18E−02	6.92E−03	3.40E−01	2.57E−02
Red Marrow	3.07E−02	2.55E−03	1.14E−01	9.75E−03
Osteogenic Cells	2.46E−02	2.10E−03	9.10E−02	7.80E−03
Skin	1.56E−02	1.31E−03	5.76E−02	4.88E−03
Spleen	3.48E−02	2.94E−03	1.29E−01	1.08E−02
Thymus	1.35E−01	1.37E−02	4.98E−01	5.19E−02
Thyroid	1.50E−02	1.70E−03	5.53E−02	6.32E−03
Bladder Wall	7.57E−03	8.46E−04	2.80E−02	3.13E−03
Uterus	1.23E−02	1.12E−03	4.56E−02	4.13E−03
Total body	4.24E−02	3.30E−03	1.57E−01	1.23E−02